A Universal Damping Mechanism of Quantum Vibrations in Deep Sub-Barrier Fusion Reactions

Takatoshi Ichikawa[1] and Kenichi Matsuyanagi[1,2]

[1]*Yukawa Institute for Theoretical Physics, Kyoto University, Kyoto 606-8502, Japan*
[2]*RIKEN Nishina Center, Wako 351-0198, Japan*

(Dated: June 29, 2015)

We demonstrate the damping of quantum octupole vibrations near the touching point when two colliding nuclei approach each other in the mass-asymmetric ^{208}Pb + ^{16}O system, for which the strong fusion hindrance was clearly observed. We, for the first time, apply the random-phase approximation method to the heavy-mass asymmetric di-nuclear system to calculate the transition strength B(E3) as a function of the center-of-mass distance. The obtained B(E3) strengths are substantially damped near the touching point, because the single-particle wave functions of the two nuclei strongly mix with each other and a neck is formed. The energy-weighted sums of B(E3) are also strongly correlated with the damping factor which is phenomenologically introduced in the standard coupled-channel calculations to reproduce the fusion hindrance. This strongly indicates that the damping of the quantum vibrations universally occurs in the deep sub-barrier fusion reactions.

PACS numbers: 21.60.Ev, 24.10.Eq, 25.70.Jj

Heavy-ion fusion reactions are an excellent probe to investigate the fundamental features of the dynamics for many-body quantum systems. When a projectile approaches a target, the Coulomb barrier is formed, because of the strong cancellation between the Coulomb repulsion and the nuclear attractive force. Nuclear fusion takes place when the projectile penetrates through this Coulomb barrier. At incident energies in the vicinity of the Coulomb barrier height, called the sub-barrier fusion, the strong enhancements of fusion cross sections, compared to the estimations of a simple one-dimensional potential model, have been observed in many systems. These enhancements are well accounted for in terms of the couplings between the relative motion of the colliding nuclei and the intrinsic degrees of freedom such as collective vibrations of the target and the projectile [1]. The coupled channel (CC) model, which takes into account this mechanism, has been successful in describing such enhancements [2, 3].

Recent experiments at extremely low incident energies, called the deep sub-barrier energies, revealed, however, that steep falloffs of the fusion cross sections, compared to the estimations of the standard CC model, emerge in a wide range of mass systems [4, 5] (see Ref. [6] for details). These steep falloff phenomena are often called the fusion hindrance. An important quantity for understanding this fusion hindrance is the potential energy at the touching point of the colliding nuclei, which is strongly correlated with the threshold incident energy for the emergence of the fusion hindrance. That is, the fusion hindrance would be associated with the dynamics in the overlap region of the two colliding nuclei (see Fig. 1 in Ref. [7]).

A theoretical challenge is how to extend the standard CC model to describe these fusion hindrance phenomena in the overlap region. Two different models based on assumptions opposite to each other have been proposed [6]. One is the sudden approach proposed by Mişicu and Esbensen [8, 9]. They constructed a heavy ion-ion potential with a shallow potential pocket considering the Pauli principle effect acting when two colliding nuclei overlap with each other. The other is the adiabatic approach proposed by Ichikawa *et al.* [10]. In this approach, neck formations between the colliding nuclei are taken into account in the overlap region. Based on this picture, the sudden and adiabatic processes were smoothly jointed by phenomenologically introducing the damping factor in the coupling form factor [11]. Later, we showed that the physical origin of the damping factor is the damping of quantum vibrations of the target and the projectile near the touching point using the random-phase approximation (RPA) method for the light mass-symmetric ^{16}O + ^{16}O and ^{40}Ca + ^{40}Ca systems [12].

In this Letter, we show that the damping of the quantum vibrations near the touching point is a universal mechanism in the deep sub-barrier fusions and is responsible for the fusion hindrance. A typical example optimally suited for this purpose is the recent precise data for the ^{208}Pb + ^{16}O fusion [5]. The performances of both the sudden and adiabatic models have been well tested in this system [9, 11]. The adiabatic model can reproduce well the experimental data rather than the sudden model for the fusion hindrance. To discriminate which model is a better description, we here show the physical origin of the damping factor introduced in Ref. [11] in the heavy-mass asymmetric ^{208}Pb + ^{16}O system.

In the standard CC model (and the sudden model), the vibrational modes of the individual colliding nuclei are assumed not to change, even when the two nuclei strongly overlap with each other. However, as shown in Ref. [12], the single-particle wave functions are drastically changed by level repulsions, which are associated with the neck formations. We apply the RPA method to the heavy-mass asymmetric system, ^{208}Pb + ^{16}O, and show that these mechanisms lead to damping of quantum vibrations in the

colliding nuclei near the touching point. This is exhibited by a drastic decreases of the B(E3) strengths carried by low-energy RPA excitation modes.

To illustrate our main idea, we first discuss the Nilsson diagram for protons as a function of the center-of-mass distance, R, in the ^{208}Pb + ^{16}O system. We calculate the mean-field potential for the ^{208}Pb + ^{16}O system using the folding procedure with the single Yukawa function [13]. Before the touching point, we assume the spherical shape for both nuclei. After the touching point, we describe the nuclear shapes with the reflection-asymmetric lemniscatoids parametrization [14]. (The parametrization dependence is negligible, because in this Letter we do not discuss the strongly overlapping region.) Based on these densities, we also calculate the Coulomb potential. We use the radius for the proton and neutron potentials, R_0, with $R_0 = 1.27A^{1/3}$ fm, where A is the total nucleon number. The depths of the neutron and proton potentials for individual ^{16}O and ^{208}Pb nuclei, V_T and V_P, are taken from Ref. [15]. In the folding procedure, we smoothly joint the two different depth parameters of the mean-field potentials for ^{18}O and ^{208}Pb by the function $V_0(z) = \frac{1}{2}\left[(V_T - V_P)\cdot \mathrm{erf}\{(z-z_c)/\mu\} + (V_T + V_P)\right]$, where z_c denotes the center position between the two surfaces of the colliding nuclei and μ denotes the smoothing parameter. We take $\mu = 0.8$ fm, which is the same as the diffuseness parameter of the single-particle potential. In the calculations, the origin is located at the center-of-mass position of the two nuclei.

Using the obtained mean-field potentials, we solve the axially-symmetric Schrödinger equation with the spin-orbit force. The details of the model and the parameters are similar to Refs. [13, 15]. Then, the z component of the total angular momentum, Ω, is the good quantum number. Note that the parity is not a good quantum number because the mean-field potential for the whole system breaks the space-reflection symmetry. We expand the single-particle wave functions in terms of the deformed harmonic-oscillator bases in the cylindrical coordinate representation. The deformation parameter of the basis functions is determined so as to cover the target and the projectile. The basis functions with energies lower than 26 $\hbar\omega$ are taken into account.

Figure 1 shows the Nilsson diagram as a function of the center-of-mass distance R. In the figure, we can see extremely strong Coulomb effect of ^{208}Pb on ^{16}O. The single-particle $p_{1/2}$ and $p_{3/2}$ states in ^{16}O are shown by the (red) thick solid lines. Even at the large separation distance $R = 20$ fm, the energies of these two states are higher than the Fermi energy of the $s_{1/2}$ state in ^{208}Pb. The miss-match of the two Fermi levels between ^{16}O and ^{208}Pb occurs due to the strong Coulomb effect. At an infinite separation distance, the energies of the $p_{1/2}$ and $p_{3/2}$ states for ^{16}O are -5.88 and -10.7 MeV, respectively. Thus, at $R = 20$ fm, the depth of the mean-field potential for ^{16}O becomes shallow by about 5 MeV due to the Coulomb effect from ^{208}Pb.

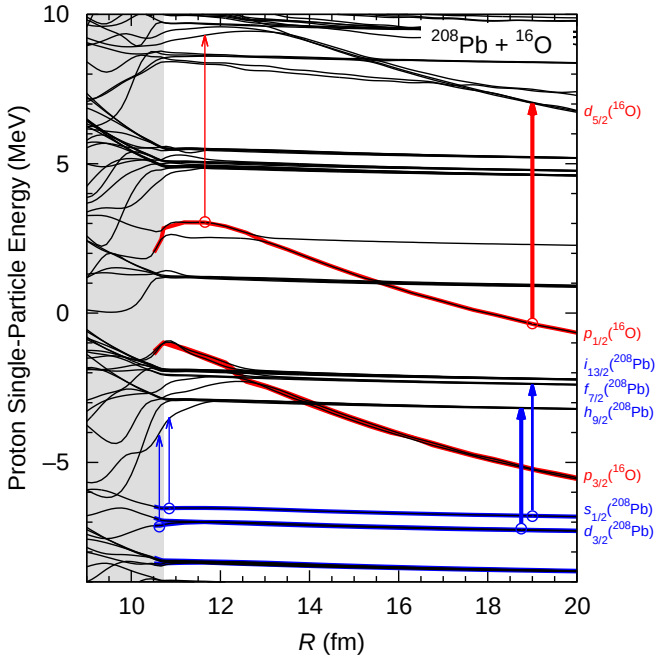

FIG. 1. (Color online) Nilsson diagram for the ^{208}Pb + ^{16}O syatem as a function of R. The light gray (red) thick lines represent the occupied $p_{1/2}$ and $p_{3/2}$ states in ^{16}O. The dark gray (blue) thick solid lines show the occupied states in ^{208}Pb. The gray area indicates the overlap region of the colliding nuclei. The arrows represent the main particle-hole excitations constituting the RPA modes.

The single-particle energies of the $p_{1/2}$ and $p_{3/2}$ states in ^{16}O remarkably increase with decreasing R due to the increasing Coulomb effect from ^{208}Pb. Then, many level crossings and repulsions between the energy levels of ^{16}O and ^{208}Pb occur. With decreasing R, the energy of the $p_{1/2}$ state becomes positive around $R = 18$ fm, that is, it changes into a *resonance* state, but there is still a sufficiently high Coulomb barrier. After that, it goes across the $f_{5/2}$ and $p_{3/2}$ states of ^{208}Pb around $R = 16$ fm and the $p_{1/2}$ state of ^{208}Pb around $R = 13$ fm. Below $R = 13$ fm, the Coulomb barrier becomes lower due to the attractive nuclear mean-field potential. Then, the strong mixture of the single-particle states between ^{16}O and ^{208}Pb starts in many levels, which causes many level splittings seen in the Nilsson diagram.

We now solve the RPA equation at each R for the mass-asymmetric ^{208}Pb + ^{16}O system. We calculate the first excited 3^- (octupole vibrational) states of ^{16}O and ^{208}Pb, which give the main contributions in the standard CC calculations. We can easily apply the RPA method to the di-nuclear system, because its the wave function is described with a one-center Slater determinant. We take the single-particle levels for each neutron and proton up to 200th and the coherent superposition of all one-particle one-hole states with excitation energies below 30 MeV. We follow the diabatic single-particle configuration corresponding to the ground state of ^{16}O. The occupied $p_{1/2}$ and $p_{3/2}$ states

in ^{16}O are represented by the light gray (red) thick curves in Fig. 1. We carry out the RPA calculation avoiding immediate vicinities of the level-crossing points. We use the density-dependent residual interaction taken from Ref. [16] and tune it so that the energy of the spurious center-of-mass motion becomes zero. We calculate B(E3) values for the RPA solutions with $\Omega = 0$ in individual nuclei using the shifted octupole operator, $\widehat{Q}_{30}(R - R'_0)$, where R'_0 is the center-of-mass position of the projectile or target nucleus.

At the large separation distance $R = 20$ fm, we obtain the first 3^- excited states of individual nuclei. The obtained energies and B(E3, $3^-_1 \rightarrow 0^+_1$) values are 2.86 MeV and $7.13\times10^4\ e^2\cdot\mathrm{fm}^6$ for ^{208}Pb and 4.64 MeV and $124\ e^2\cdot\mathrm{fm}^6$ for ^{16}O. The obtained transition densities and currents for the first 3^- states of ^{16}O and ^{208}Pb are depicted in Figs. 2 (a) and (c). At $R = 20$ fm, these modes are isolated. When the two nuclei approach each other, however, these modes start to fragment into several states. To evaluate the octupole collective strengths carried by low-energy excitations, we then calculate the energy-weighted sum of B(E3) strengths. By checking the spectrum of all obtained RPA modes as a function of R, we determined to take the sum for octupole excitations with $E \leq 4$ MeV and $E \leq 6$ MeV for ^{208}Pb and ^{16}O, respectively.

Figure 3 shows the B(E3) strengths for (a) ^{16}O and (b) ^{208}Pb as functions of R. The calculated values (the solid circles) drastically decrease near the touching point (the boundary between the white and gray areas) in both nuclei. The transition densities and currents for the RPA modes with the maximum B(E3) at the touching point are depicted in Fig. 2 (b) and (d). These figures indicate that the octupole collectivities of both ^{16}O and ^{208}Pb are considerably diminished by each colliding partner.

The microscopic origin of the damping of these vibrations is easily seen as follows. At $R = 20$ fm, the main proton components of the 3^- modes are the excitations $p_{1/2} \rightarrow d_{5/2}$ and $p_{3/2} \rightarrow d_{5/2}$ for ^{16}O, and the excitations $d_{3/2} \rightarrow h_{9/2}$ and $s_{1/2} \rightarrow f_{7/2}$ for ^{208}Pb [see the (red and blue) arrows around $R = 19$ fm in Fig. 1]. The density distributions of the $p_{1/2}$ and $d_{5/2}$ states in ^{16}O are displayed in (a) and (b) of Fig. 4. Their wave functions suffer major modifications near the touching point at $R = 11.65$ fm, as depicted in (c) and (d) of Fig. 4 [see also the (red) arrow at $R = 11.65$ fm in Fig. 1]. We can clearly see the neck formations in (d). Also for ^{208}Pb, similar drastic changes of single-particle wave functions occur for both protons and neutrons near the Fermi surface, causing the damping of the collectivity of the 3^- vibration [see the (blue) arrows around 10.6 fm in Fig. 1].

Finally, to see the correlation with the damping factor phenomenologically introduced in the CC calculation, we compare the calculated results with the damping factor that well reproduced the experimental data of the fusion cross section for ^{208}Pb + ^{16}O [11]. The damping factor is given by $\Phi(r, \lambda_\alpha) = e^{-(r-R_d-\lambda_\alpha)^2/2a_d^2}$ for $r < R_d + \lambda_\alpha$ (otherwise

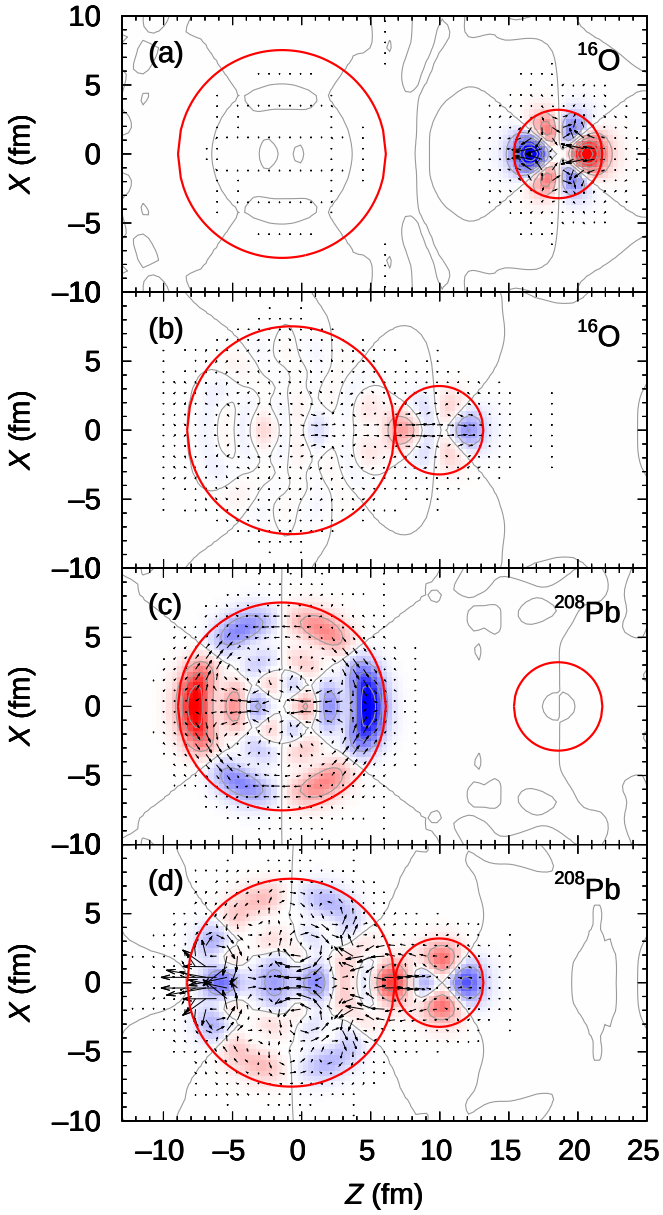

FIG. 2. (Color online) Contour maps of the proton transition densities and current distributions for the first excited 3^- states of ^{16}O and ^{208}Pb at $R = 20$ and 10.73 fm. The contour lines correspond to multiples of 0.01 fm^{-2} and 0.005 fm^{-2} for ^{16}O and ^{208}Pb, respectively. The arrows represent the current density. The currents and colors are normalized at $R = 20$ fm in individual nuclei. The (red) thick solid circles indicate the half depth of the mean-field potential.

$\Phi = 1$), where a_d and λ_a denote the damping width and the eigenvalues of the coupling matrix elements, respectively. The parameter R_d is given by $R_d = r_d(A_T^{1/3} + A_P^{1/3})$, where r_d denotes the damping radius parameter, and A_T and A_P the mass numbers of the target and the projectile, respectively. In the calculation of Ref. [11], $r_d = 1.298$ fm and $a_d = 1.05$ fm are used. Then, the largest eigenvalue of λ_α is 1.46 fm. In Figs. 3 (a) and (b), the dashed curves represent the damp-

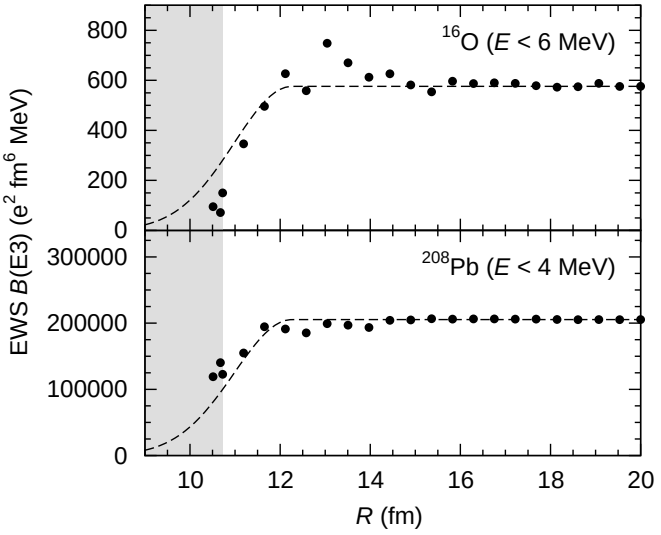

FIG. 3. Energy-weighted sums of B(E3) for (a) ^{16}O and (b) ^{208}Pb as functions of R. The solid circles show the results of the RPA calculations. The dashed curves represent the damping factor which well reproduces the experimental data of the fusion cross section for ^{208}Pb + ^{16}O taken from Ref. [11]. The gray area indicates the overlap region of the colliding nuclei.

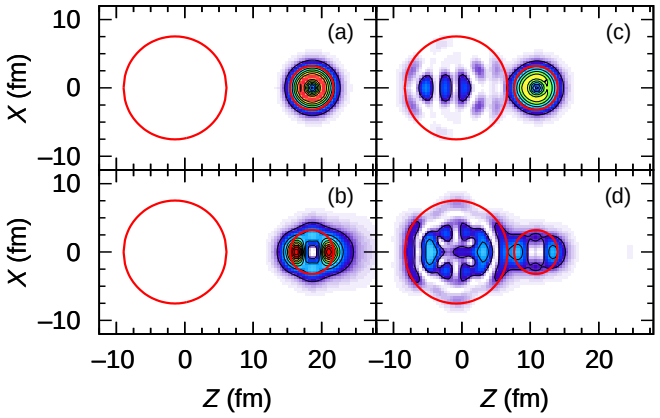

FIG. 4. (Color online) Density distributions of the $p_{1/2}$ and $d_{5/2}$ states originally belonging to ^{16}O at R = 20 fm and their evolutions at R = 11.65 fm. The (red) thick solid circles indicate the half depth of the mean-field potential. The contour lines correspond to multiples of 0.0015 fm^{-3}. The colors are normalized at 0.01 fm^{-3}.

ing factor with these parameters normalized at R = 20 fm. We can see that the damping factor strongly correlates with the calculated energy-weighted sums of B(E3) in the low-energy region, which clearly indicates that the damping of the quantum vibrations indeed occurs when the colliding nuclei approach each other.

In summary, we have demonstrated the damping of the quantum octupole vibrations of both ^{16}O and ^{208}Pb, when they approach each other. To show this, we, for the first time, applied the RPA method to the heavy mass-asymmetric ^{208}Pb + ^{16}O system. We have discussed the Nilsson diagram as a function of the center-of-mass distance R and have shown that the single-particle energies in ^{16}O are largely sifted to the positive-energy direction by the strong Coulomb effects from the heavy-mass ^{208}Pb in a colliding process. We calculated the B(E3) strengths for ^{16}O and ^{208}Pb as a function of R. The obtained B(E3) strengths are substantially damped near the touching point of the colliding nuclei. The obtained energy-weighted sum of B(E3) in the low-energy region exhibits a strong correlation with the damping factor that reproduces well the experimental data of the fusion cross section for ^{208}Pb + ^{16}O. This is a clear evidence that the damping of the quantum octupole vibrations indeed occur near the touching point in the deep sub-barrier fusion reactions. The drastic change of single-particle wave functions consitituting the low-energy collective excitations discussed in this paper would commonly occur in all deep sub-barrier reactions. Therefore, the damping of quantum vibrations in both the target and the projectile near the touching point seems to be a universal mechanism causing the fusion hindrance, which should be taken into account in the standard CC model.

A part of this research was funded by the MEXT HPCI STRATEGIC PROGRAM. This work was supported by JPSJ KAKENHI Grant Number 15K05078.

[1] M. Dasgupta *et al.*, Annu. Rev. Nucl. Part. Sci. **48**, 401 (1998).
[2] A. B. Balantekin and N. Takigawa, Rev. Mod. Phys. **70**, 77 (1998).
[3] K. Hagino and N. Takigawa, Prog. Theor. Phys. **128**, 1061 (2012).
[4] C. L. Jiang *et al.*, Phys. Rev. Lett. **89**, 052701 (2002); **93**, 012701 (2004); Phys. Rev. C **73**, 014613 (2006); **75**, 057604 (2007); Phys. Rev. Lett. **113**, 022701 (2014).
[5] M. Dasgupta *et al.*, Phys. Rev. Lett. **99**, 192701 (2007).
[6] B.B. Back *et al.*, Rev. Mod. Phys. **86**, 317 (2014).
[7] T. Ichikawa, K. Hagino, and A. Iwamoto, Phys. Rev. C **75**, 064612 (2007).
[8] Ş Mişicu and H. Esbensen, Phys. Rev. Lett. **96**, 112701 (2006); Phys. Rev. C **75**, 034606 (2007).
[9] H. Esbensen and Ş Mişicu, Phys. Rev. C **76**, 054609 (2007).
[10] T. Ichikawa, K. Hagino, and A. Iwamoto, Phys. Rev. C **75**, 057603 (2007).
[11] T. Ichikawa, K. Hagino, A. Iwamoto, Phys. Rev. Lett. **103**, 202701 (2009); EPJ Web Conf. **17**, 07001 (2011).
[12] T. Ichikawa, K. Matsuyanagi, Phys. Rev. C **88**, 011602(R) (2013).
[13] M. Bolsterli *et al.*, Phys. Rev. C **5** 1050 (1972).
[14] G. Royer and B. Remaud, Nucl. Phys. **A444**, 477 (1985).
[15] P. Möller *et al.*, At. Data Nucl. Data Tables **59** (1995) 185.
[16] S. Shlomo and G. Bertsch, Nucl. Phys. **A 243**, 507 (1975).